Position USBL/DVL sensor-based navigation filter in the presence of unknown ocean currents

Marco Morgado, Pedro Batista, Paulo Oliveira, and Carlos Silvestre

Automatica, vol. 47, no. 12, pp. 2604-2614, December 2011

https://doi.org/10.1016/j.automatica.2011.09.024

Position USBL/DVL Sensor-based Navigation Filter in the presence of Unknown Ocean Currents ⋆

M. Morgado, P. Batista, P. Oliveira, and C. Silvestre

Institute for Systems and Robotics, Instituto Superior Técnico, Av. Rovisco Pais, 1, 1049-001, Lisbon, Portugal

Abstract

This paper presents a novel approach to the design of globally asymptotically stable (GAS) position and velocity filters for Autonomous Underwater Vehicles (AUVs) based directly on the sensor readings of an Ultra-short Baseline (USBL) acoustic array system and a Doppler Velocity Log (DVL). The proposed methodology is based on an equivalent linear time-varying (LTV) system that fully captures the dynamics of the nonlinear system, allowing for the use of powerful linear system analysis and filtering design tools that yield GAS filter error dynamics. Numerical results using Monte Carlo simulations and comparison to the Bayesian Cramér Rao Bound (BCRB) reveal that the performance of the proposed filter is tight to this theoretical estimation error lower bound. In comparison with other approaches, the present solution achieves the same level of performance of the Extended Kalman Filter (EKF), which does not offer GAS guarantees, and outperforms other classical filtering approaches designed in inertial coordinates instead of the sensor-based coordinate frame.

Key words: Navigation systems; Performance limits; Observability; Nonlinear models; Time-varying systems; Kalman filters

1 Introduction

The design and implementation of navigation systems stands out as one of the most critical steps towards the successful operation of autonomous vehicles. The quality of the overall estimates of the navigation system dramatically influences the capability of the vehicles to perform precision-demanding tasks, see [26] and [18] for interesting and detailed surveys on underwater vehicle navigation and its relevance. This paper presents a novel approach to the design of globally asymptotically stable (GAS) position filters directly based on the acoustic array sensor readings.

Consider an underwater vehicle equipped with an Ultra-Short Baseline (USBL) underwater positioning device, a triad of orthogonally mounted rate gyros, and a Doppler Velocity Log (DVL), that moves in the presence of unknown ocean currents in a scenario that has a fixed transponder, as depicted in Fig. 1.

The USBL is composed of a small calibrated array of acoustic receivers and measures the distance between the transponder and the receivers installed on-board. Given the proximity of the sensors in the receiving array, hence the name Ultra-Short Baseline (USBL), it is capable of measuring more accurately the Range-Difference-of-Arrival (RDOA) of the acoustic waves at the receivers compared to the actual distances between the transponder and all the receivers. The DVL measures the velocity of the vehicle with respect to the fluid, and the rate gyros provide the angular velocities of the vehicle. Due to noisy measurements, unknown ocean currents, and the nonlinear nature of the range measurements, a filtering solution is required in order to correctly estimate the position of the transponder in the vehicle coordinate frame and the inertial velocity of the vehicle. Recent advances in the area of underwater navigation, based on merging the information from acoustic

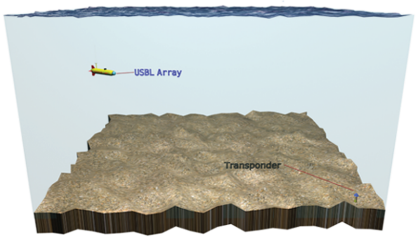

Fig. 1. Mission scenario

⋆ This paper was not presented at any IFAC meeting. Corresponding author M. Morgado. Tel. +351-21-8418054. Fax +351-21-8418092.

Email address: {marcomorgado, pbatista, pjcro, cjs}@isr.ist.utl.pt (M. Morgado, P. Batista, P. Oliveira, and C. Silvestre).

arrays and other inertial sensors like DVLs, can be found in [5,9,14,15,20,27]. Related work using nonlinear observers applied to automotive vehicles velocity estimation can be seen in [13], and references therein.

Control systems for autonomous vehicles often rely on the information provided by state observers [8,19] to perform the desired tasks. The choice of where these quantities (e.g. position, velocity, attitude, etc.) are expressed, either on body or inertial coordinate frames, depends on the purpose, application and mainly on the design methodology used to synthesise the controller. The navigation system can be designed to provide estimates expressed on any specific coordinate frame, either by posterior conversion of the outputs from one frame to another (e.g. estimator designed to provide outputs on inertial coordinates with posterior conversion to body fixed coordinates or vice-versa) or by directly designing the systems on the desired coordinate frame. Intuitively one might expect each coordinate frame tailored filter to perform better than the other on its own design frame due, for instance, to unaccounted posterior frame conversion during the filtering process. Moreover, most inertial quantities are directly sensed on the body coordinate frame, whereas for use on an inertial frame designed filter these have to be correctly converted from body to inertial coordinates, using for instance an Attitude and Heading Reference System (AHRS). Positioning devices aboard the vehicle like inverted USBL configurations obtain directly the position of transponders in body fixed coordinates, motivating the use of body referenced estimators in the design of controllers, such as homing and docking controllers, that actuate directly on the vehicles own coordinate frame.

Traditional solutions resort either to the well known Extended Kalman Filter (EKF)[17], Particle Filters (PF)[20], which lack global asymptotic stability guarantees, or to more classical filtering solutions that use a precomputed position fix from the USBL device in inertial coordinates and obtain the filtered vehicle position in a simple Linear Time-Invariant (LTI) setting. The computation of this position fix is commonly obtained using the range and bearing and elevation angles of the transponder, which resorts to a planar wave approximation of the acoustic wave arriving at the receiving array, previously used by the authors [17]. In that case, the error cannot be guaranteed to converge to zero due to the planar wave approximation. In fact, the error converges to a neighbourhood of the origin, not arbitrarily small, that depends on the planar wave approximation, and that only vanishes as the distance between the transponder and the vehicle approaches infinity. This behaviour is obviously undesirable if the vehicle is to, for instance, dock to a station or manoeuvre [11] in the vicinity of a transponder.

The main contributions of this paper are twofold: i) the design of a globally asymptotically stable sensor-based filter to estimate the position of the transponder and the ocean current that biases the DVL readings; and ii) the performance assessment of the proposed filtering structure in comparison with theoretical performance lower bounds using Monte Carlo simulations. The solution presented in the paper departs from previous approaches as the range measurements are directly embedded in the filter structure, thus avoiding the planar wave approximation, and follows related work found in [4], where single range measurements were considered and persistent excitation conditions were imposed on the vehicle motion to bear the system observable. In this paper the framework is extended to the case of having an array of receivers installed on-board the vehicle, which allows for the analysis of the overall system without any constraint on the vehicle motion. At the core of the proposed filtering framework lies a Linear Time-Varying (LTV) system that is shown to mimic the dynamics of the nonlinear system, without resorting to any degree of linearization. The LTV model is achieved through appropriate state augmentation, allowing for the use of powerful linear system analysis and filtering design tools that yield a novel estimation solution with GAS error dynamics. The work presented herein represents the first time, to the best of the authors' knowledge, that a GAS filter is designed for this problem in a sensor-based approach, in which the nonlinear ranging observations from a single source to multiple receivers installed on-board a robotic platform, are directly used in the filtering process and not explicitly inverted to obtain a relative position fix.

The paper is organized as follows: Section 2 sets the problem framework and definitions. The proposed filter design and main contributions of the paper are presented in Section 3, where the filter structure is brought to full detail and an extensive and constructive observability analysis is carried out. An overview of the Bayesian Cramér Rao Bound (BCRB) and performance bounds is also carried out in Section 3. Monte Carlo simulation results and performance comparison with traditional solutions and the BCRB are discussed in Section 4, and finally Section 5 provides some concluding remarks.

2 Problem framework

In order to set the design framework, let $\{I\}$ denote an inertial reference coordinate frame and $\{B\}$ a coordinate frame attached to the vehicle, usually denominated as body-fixed coordinate frame. The position of the transponder $\mathbf{r}(t) \in \mathbb{R}^3$ in the vehicle coordinate frame $\{B\}$ is given by

$$ {}^{B}\mathbf{r}(t) = \mathcal{R}^T(t)({}^{I}\mathbf{s} - {}^{I}\mathbf{p}(t)), \tag{1} $$

where ${}^{I}\mathbf{s} \in \mathbb{R}^3$ is the position of the transponder in inertial coordinates, ${}^{I}\mathbf{p}(t) \in \mathbb{R}^3$ is the position of the vehicle in inertial coordinates, and $\mathcal{R}(t) \in SO(3)$ is the rotation matrix from $\{B\}$ to $\{I\}$, $SO(3)$ denotes the special orthogonal group of rotation matrices, and the operator $(\cdot)^T$ denotes the usual matrix transpose operation. The time derivative of $\mathcal{R}(t)$ verifies $\dot{\mathcal{R}}(t) = \mathcal{R}(t)\mathcal{S}(\omega(t))$, where $\omega(t) \in \mathbb{R}^3$ is the angular velocity of $\{B\}$ with respect to $\{I\}$, expressed in body-fixed coordinates, and $\mathcal{S}(\omega(t))$ is the skew-symmetric matrix that represents the cross product such that $\mathcal{S}(\omega)\, a = \omega \times a$.

Differentiating (1) in time yields

$$ {}^{B}\dot{\mathbf{r}}(t) = -\mathcal{S}\left(\omega(t)\right) {}^{B}\mathbf{r}(t) - {}^{B}\mathbf{v}(t), \tag{2} $$

where ${}^{B}\mathbf{v}(t) \in \mathbb{R}^3$ is the vehicle velocity expressed in body-fixed coordinates. The readings of the DVL are modelled by

$$ {}^{B}\mathbf{v}_{\mathbf{r}}(t) = {}^{B}\mathbf{v}(t) - \mathcal{R}^{T}(t) {}^{I}\mathbf{v}_{\mathbf{c}}(t), \tag{3} $$

where ${}^{B}\mathbf{v}_{\mathbf{r}}(t) \in \mathbb{R}^3$ is the velocity reading provided by the DVL, and ${}^{I}\mathbf{v}_{\mathbf{c}}(t) \in \mathbb{R}^3$ is the current velocity expressed in inertial coordinates and considered to be constant, that is, ${}^{I}\dot{\mathbf{v}}_{\mathbf{c}}(t) = \mathbf{0}$. Using the current velocity expressed in body-fixed coordinates ${}^{B}\mathbf{v}_{\mathbf{c}}(t) = \mathcal{R}^{T}(t) {}^{I}\mathbf{v}_{\mathbf{c}}(t)$ together with (3) in (2) yields

$$ {}^{B}\dot{\mathbf{r}}(t) = -\mathcal{S}\left(\omega(t)\right) {}^{B}\mathbf{r}(t) - {}^{B}\mathbf{v}_{\mathbf{c}}(t) - {}^{B}\mathbf{v}_{\mathbf{r}}(t). \tag{4} $$

The distances between the transponder and the receivers installed on-board the vehicle (as measured by the USBL) can be written as

$$ \rho_i(t) = \| {}^{B}\mathbf{b}_i - {}^{B}\mathbf{r}(t) \|, \quad i = 1, \ldots, n_r, \tag{5} $$

where ${}^{B}\mathbf{b}_i \in \mathbb{R}^3$ denotes the position of the receiver in $\{B\}$ and n_r is the number of receivers on the USBL. For the sake of clarity of presentation, the superscript ${}^{B}(\cdot)$ denoting the body-fixed coordinate frame will be omitted as follows

$$ \begin{aligned} \mathbf{r}(t) &:= {}^{B}\mathbf{r}(t), & \mathbf{v}_{\mathbf{r}}(t) &:= {}^{B}\mathbf{v}_{\mathbf{r}}(t) \\ \mathbf{v}_{\mathbf{c}}(t) &:= {}^{B}\mathbf{v}_{\mathbf{c}}(t), & \mathbf{b}_i &:= {}^{B}\mathbf{b}_i \end{aligned} $$

Thus, combining the time-derivative of $\mathbf{v}_{\mathbf{c}}(t)$ with (4) and (5) yields the nonlinear system

$$ \begin{cases} \dot{\mathbf{r}}(t) = -\mathcal{S}\left(\omega(t)\right) \mathbf{r}(t) - \mathbf{v}_{\mathbf{c}}(t) - \mathbf{v}_{\mathbf{r}}(t), \\ \dot{\mathbf{v}}_{\mathbf{c}}(t) = -\mathcal{S}\left(\omega(t)\right) \mathbf{v}_{\mathbf{c}}(t), \\ \rho_i(t) = \| \mathbf{b}_i - \mathbf{r}(t) \|, \; i = 1, \ldots, n_r. \end{cases} \tag{6} $$

The problem addressed in this paper, the quantities to be estimated and filtered, and the considered measurements can be summarized in the following statement.

Problem statement 1 *Consider a robotic vehicle that is equipped with a fluid relative velocity sensor, a triad of orthogonally mounted rate gyros, and an array of acoustic receivers that provide multiple range measurements to a fixed transponder in the mission operation scenario. Design a filter or state observer for the transponder position* $\mathbf{r}(t)$ *and the ocean current velocity* $\mathbf{v}_{\mathbf{c}}(t)$ *described in* (6)*, considering noisy measurements for the vehicle angular velocity* $\omega(t)$*, the fluid relative velocity* $\mathbf{v}_{\mathbf{r}}(t)$*, and the ranges* $\rho_i(t)$*, with* $i = 1, \ldots, n_r$*, as summarized in Table 1.*

Table 1
Summary of measured quantities and variables to be estimated

Estimate	Measure
Transponder pos. - $\mathbf{r}(t)$	Relative vel. to fluid - $\mathbf{v}_{\mathbf{r}}(t)$
Current vel. $\mathbf{v}_{\mathbf{c}}(t)$	Angular vel. - $\omega(t)$
(in body-fixed coord.)	Ranges - $\rho_i(t)$, $i = 1, \ldots, n_r$

3 Filter design

In this section the main results and contributions of the paper are presented. In order to reduce the complexity of the system dynamics a Lyapunov state transformation is firstly introduced in Section 3.1. The LTV system that will mimic the nonlinear behaviour of the original system (6) is proposed in Section 3.2, by means of an appropriate state augmentation. The observability analysis of the LTV system and its relation with the original nonlinear system is conducted in Section 3.3, and finally in Section 3.4, the design of a Kalman filter is proposed in a stochastic setting for the resulting system. In the course of the filter design, the augmented LTV system is shown to be uniformly completely observable, a sufficient condition for a LTV Kalman filter to yield GAS estimation error dynamics. An overview of theoretical performance lower bounds with application to the problem at hand is carried out in Section 3.5.

3.1 State transformation

Consider the following state transformation

$$ \begin{bmatrix} \mathbf{x}_{\mathbf{1}}(t) \\ \mathbf{x}_{\mathbf{2}}(t) \end{bmatrix} := \mathbf{T}(t) \begin{bmatrix} \mathbf{r}(t) \\ \mathbf{v}_{\mathbf{c}}(t) \end{bmatrix}, \tag{7} $$

where $\mathbf{T}(t) := \operatorname{diag}\left(\mathcal{R}(t), \mathcal{R}(t)\right)$ is a Lyapunov state transformation which preserves all observability properties of the original system [6]. The new system dynamics are given by

$$ \begin{cases} \dot{\mathbf{x}}_{\mathbf{1}}(t) = -\mathbf{x}_{\mathbf{2}}(t) - \mathbf{u}(t), \\ \dot{\mathbf{x}}_{\mathbf{2}}(t) = \mathbf{0}, \\ \rho_i(t) = \| \mathbf{b}_i - \mathcal{R}^{T}(t) \mathbf{x}_{\mathbf{1}}(t) \|, \quad i = 1, \ldots, n_r, \end{cases} \tag{8} $$

where $\mathbf{u}(t) = \mathcal{R}(t) \mathbf{v}_{\mathbf{r}}(t)$. The advantage of considering this state transformation is that the new unforced system dynamics becomes highly simplified as time-invariant, although the system output becomes time-varying and is still nonlinear.

3.2 State augmentation

In order to derive a linear system equivalent to the original nonlinear system, a state augmentation procedure follows inherited directly from the kinematics of the nonlinear range outputs of (8). Thus, taking the time-derivative of $\rho_i(t)$ in

(8) yields

$$\dot{\rho}_i(t) = \frac{1}{\rho_i(t)} \left[(\mathbf{b}_i^T \mathcal{S}(\omega(t)) \mathcal{R}^T(t) - \mathbf{u}^T(t)) \mathbf{x_1}(t) + \mathbf{b}_i^T \mathcal{R}^T(t) \mathbf{x_2}(t) - \mathbf{x_1}^T(t) \mathbf{x_2}(t) + \mathbf{b}_i^T \mathcal{R}^T(t) \mathbf{u}(t) \right]. \quad (9)$$

Identifying the nonlinear term $\mathbf{x_1}^T(t)\mathbf{x_2}(t)$ in (9) leads to the creation of the augmented states that will mimic this non-linearity: $x_{n_r+3}(t) := \mathbf{x_1}^T(t)\mathbf{x_2}(t)$ and $x_{n_r+4}(t) := \|\mathbf{x_2}(t)\|^2$, with the corresponding kinematics $\dot{x}_{n_r+3}(t) = -\mathbf{u}^T(t)\mathbf{x_2}(t) - x_{n_r+4}(t)$ and $\dot{x}_{n_r+4}(t) = \mathbf{0}$.

Thus a new dynamic system is created by augmenting the original nonlinear system with the states

$$\begin{cases} x_3(t) := \rho_1(t), \ \ldots\ldots, & x_{n_r+2}(t) := \rho_{n_r}(t), \\ x_{n_r+3}(t) := \mathbf{x_1}^T(t)\mathbf{x_2}(t), & x_{n_r+4}(t) := \|\mathbf{x_2}(t)\|^2, \end{cases}$$

and denoting the new augmented state vector $\mathbf{x}(t) \in \mathbb{R}^{8+n_r}$ by $\mathbf{x}(t) = \left[\mathbf{x_1}^T(t)\ \mathbf{x_2}^T(t)\ x_3(t)\ \ldots\ x_{n_r+2}(t)\ x_{n_r+3}(t)\ x_{n_r+4}(t) \right]^T$. Combining the new augmented states dynamics with (8) it is easy to verify that the augmented dynamics can be written as

$$\dot{\mathbf{x}}(t) = \mathbf{A}(t)\mathbf{x}(t) + \mathbf{B}(t)\mathbf{u}(t),$$

where

$$\mathbf{B}(t) = \left[-\mathbf{I}_3\ \mathbf{0}\ \frac{\mathcal{R}(t)\mathbf{b}_1}{\rho_1(t)}\ \cdots\ \frac{\mathcal{R}(t)\mathbf{b}_{n_r}}{\rho_{n_r}(t)}\ \mathbf{0}\ \mathbf{0} \right]^T \quad (10)$$

and

$$\mathbf{A}(t) = \begin{bmatrix} \mathbf{0} & -\mathbf{I} & \mathbf{0} & \mathbf{0} & \mathbf{0} \\ \mathbf{0} & \mathbf{0} & \mathbf{0} & \mathbf{0} & \mathbf{0} \\ \frac{(\mathbf{b}_1^T \mathcal{S}(\omega(t)) \mathcal{R}^T(t) - \mathbf{u}^T(t))}{\rho_1(t)} & \frac{\mathbf{b}_1^T \mathcal{R}^T(t)}{\rho_1(t)} & \mathbf{0} & -\frac{1}{\rho_1(t)} & 0 \\ \vdots & \vdots & \vdots & \vdots & \vdots \\ \frac{(\mathbf{b}_{n_r}^T \mathcal{S}(\omega(t)) \mathcal{R}^T(t) - \mathbf{u}^T(t))}{\rho_{n_r}(t)} & \frac{\mathbf{b}_{n_r}^T \mathcal{R}^T(t)}{\rho_{n_r}(t)} & \mathbf{0} & -\frac{1}{\rho_{n_r}(t)} & 0 \\ \mathbf{0} & -\mathbf{u}^T(t) & \mathbf{0} & 0 & -1 \\ \mathbf{0} & \mathbf{0} & \mathbf{0} & 0 & 0 \end{bmatrix}. \quad (11)$$

The following assumption is required so that (10) and (11) are well defined.

Assumption 2 *The motion of the vehicle is such that*

$$\begin{array}{lll} \exists & \forall & : R_{min} \leq \rho_i(t) \leq R_{max}. \\ R_{min} > 0 & t \geq t_0 & \\ R_{max} > 0 & i = 1, \ldots, n_r & \end{array}$$

From a practical point of view this is not restrictive since the vehicle will never be on top of a transponder, nor arbitrarily far away from it. Note that the RDOA at the receivers are considered to be measured more accurately compared to the absolute distance between the transponder and any given reference receiver of the USBL. Selecting a reference sensor on the array, for instance receiver 1 for now, all the other ranges are easily reconstructed from the range measured at receiver 1 and the RDOA between receiver 1 and the other receivers, that is $\rho_j(t) = \rho_1(t) - \delta\rho_{1_j}(t)$, where $\delta\rho_{1_j}(t) = \rho_1(t) - \rho_j(t)$.

Taking into account that the augmented states $x_3(t), \ldots, x_{n_r+2}(t)$ that correspond to the ranges are actually measured, it is straightforward to show from the outputs of (6) that

$$\rho_i^2(t) - \rho_j^2(t) = \|\mathbf{b}_i\|^2 - \|\mathbf{b}_j\|^2 - 2(\mathbf{b}_i - \mathbf{b}_j)^T \mathcal{R}^T(t)\mathbf{x_1}(t),$$

which leads to

$$\frac{2(\mathbf{b}_i - \mathbf{b}_j)^T \mathcal{R}^T(t)\mathbf{x_1}(t)}{\rho_i(t) + \rho_j(t)} + \rho_i(t) - \rho_j(t) = \frac{\|\mathbf{b}_i\|^2 - \|\mathbf{b}_j\|^2}{\rho_i(t) + \rho_j(t)},$$

or, equivalently,

$$\frac{2(\mathbf{b}_i - \mathbf{b}_j)^T \mathcal{R}^T(t)\mathbf{x_1}(t)}{\rho_i(t) + \rho_j(t)} + x_{2+i}(t) - x_{2+j}(t) = \frac{\|\mathbf{b}_i\|^2 - \|\mathbf{b}_j\|^2}{\rho_i(t) + \rho_j(t)}, \quad (12)$$

where the right hand-side of (12) is measured and the left hand-side is linear on the system state.

In order to complete the augmented system dynamics, discarding the original nonlinear outputs in (8), and considering (12), define the new augmented system outputs $\mathbf{y}(t) \in \mathbb{R}^{n_r+n_c}$ as

$$\mathbf{y}(t) = \begin{bmatrix} \left[x_3(t)\ x_3(t) - x_4(t)\ \cdots\ x_3(t) - x_{2+n_r}(t) \right]^T \\ \frac{2(\mathbf{b}_1 - \mathbf{b}_2)^T \mathcal{R}^T(t)\mathbf{x_1}(t)}{\rho_1(t) + \rho_2(t)} + x_{2+1}(t) - x_{2+2}(t) \\ \frac{2(\mathbf{b}_1 - \mathbf{b}_3)^T \mathcal{R}^T(t)\mathbf{x_1}(t)}{\rho_1(t) + \rho_3(t)} + x_{2+1}(t) - x_{2+3}(t) \\ \vdots \\ \frac{2(\mathbf{b}_{n_r-2} - \mathbf{b}_{n_r})^T \mathcal{R}^T(t)\mathbf{x_1}(t)}{\rho_{n_r-2}(t) + \rho_{n_r}(t)} + x_{2+n_r-2}(t) - x_{2+n_r}(t) \\ \frac{2(\mathbf{b}_{n_r-1} - \mathbf{b}_{n_r})^T \mathcal{R}^T(t)\mathbf{x_1}(t)}{\rho_{n_r-1}(t) + \rho_{n_r}(t)} + x_{2+n_r-1}(t) - x_{2+n_r}(t) \end{bmatrix},$$

where $n_c = C_2^{n_r} = \frac{n_r!}{2(n_r-2)!} = \frac{n_r(n_r-1)}{2}$ is the number of all possible 2-combinations of n_r elements. Even tough the observability analysis presented in the sequel does not require all possible combinations to bear constructive results (a subset of these combinations might yield the overall system observable), the derivation is presented using all n_c combinations in order to exploit all available information from the acoustic array in the filtering framework.

Let

$$\begin{aligned}
\mathbf{U_r} &:= \begin{bmatrix}\mathbf{b}_1 & \cdots & \mathbf{b}_{n_r}\end{bmatrix}^T && \in \mathbb{R}^{n_r\times 3},\\
\boldsymbol{\Upsilon}(t) &:= \begin{bmatrix}\rho_1(t) & \cdots & \rho_{n_r}(t)\end{bmatrix}^T && \in \mathbb{R}^{n_r\times 1},\\
\mathbf{D}_\Upsilon(t) &:= \operatorname{diag}(\Upsilon(t)) && \in \mathbb{R}^{n_r\times n_r},\\
\mathbf{D}_{\rho+}(t) &:= \operatorname{diag}\left(\begin{bmatrix}\rho_1(t)+\rho_2(t)\\ \rho_1(t)+\rho_3(t)\\ \vdots\\ \rho_{n_r-2}(t)+\rho_{n_r}(t)\\ \rho_{n_r-1}(t)+\rho_{n_r}(t)\end{bmatrix}\right) && \in \mathbb{R}^{n_c\times n_c}.
\end{aligned}$$

In compact form, the augmented system dynamics can be written as

$$\begin{cases}\dot{\mathbf{x}}(t) = \mathbf{A}(t)\mathbf{x}(t) + \mathbf{B}(t)\mathbf{u}(t),\\ \mathbf{y}(t) = \mathbf{C}(t)\mathbf{x}(t),\end{cases} \tag{13}$$

where

$$\mathbf{C}(t) = \begin{bmatrix}\mathbf{0}_{n_r\times 3} & \mathbf{0}_{n_r\times 3} & \mathbf{C_0} & \mathbf{0}_{n_r\times 2}\\ \mathbf{C_1}(t) & \mathbf{0}_{n_c\times 3} & \mathbf{C_2} & \mathbf{0}_{n_c\times 2}\end{bmatrix},$$

$$\mathbf{C_0} = \begin{bmatrix}1 & 0 & \cdots & 0\\ 1 & -1 & & \\ \vdots & \mathbf{0} & \ddots & \mathbf{0}\\ 1 & & & -1\end{bmatrix}, \quad \mathbf{C_2} = \begin{bmatrix}1 & -1 & 0 & 0 & \cdots & 0\\ 1 & 0 & -1 & 0 & \cdots & 0\\ & & & \vdots & & \\ 0 & \cdots & 0 & 1 & 0 & -1\\ 0 & \cdots & 0 & 0 & 1 & -1\end{bmatrix},$$

and

$$\mathbf{C_1}(t) = 2\mathbf{D}_{\rho+}^{-1}(t)\mathbf{C_2}\mathbf{U_r}\mathcal{R}^T(t). \tag{14}$$

3.3 Observability analysis

The Lyapunov state transformation and the state augmentation that were carried out allowed to derive the LTV system described in (13), which ensembles the behaviour of the original nonlinear system (6). The dynamic system (13) can be regarded as a LTV, even though it might seem strange that the system matrix $\mathbf{A}(t)$ depends explicitly on the system input and output, as evidenced by (11). Nevertheless, this is not a problem from the theoretical point of view for the design of an observer, since both the input and output of the system are known continuous bounded signals, whereas for the design of a state controller this consideration would not be feasible. The idea is not new either, see, e.g., [7], and it just suggests, in this case, that the observability of (13) may be connected with the evolution of the system input or output (or both), which is not common and does not happen when this matrix does not depend on the system input or output.

In order to fully understand and couple the behaviour of both systems, the observability analysis of (13) is carried out in this section using classical linear systems theory. This analysis is conducted based on the observability Gramian associated with the pair $(\mathbf{A}(t), \mathbf{C}(t))$, which is given by [2]

$$\mathcal{W}(t_0, t_f) = \int_{t_0}^{t_f} \mathbf{\Phi}^T(t, t_0)\mathbf{C}^T(t)\mathbf{C}(t)\mathbf{\Phi}(t, t_0)dt,$$

where $\mathbf{\Phi}(t, t_0)$ is the state transition matrix of the LTV system (13).

Tedious, lengthy, but straightforward computations show that the transition matrix associated with $\mathbf{A}(t)$ is given by

$$\mathbf{\Phi}(t, t_0) = \begin{bmatrix}\mathbf{\Phi}_{AA}(t, t_0) & \mathbf{0}_{6\times n_r} & \mathbf{0}_{6\times 2}\\ \mathbf{\Phi}_{BA}(t, t_0) & \mathbf{I}_{n_r} & \mathbf{\Phi}_{BC}(t, t_0)\\ \mathbf{\Phi}_{CA}(t, t_0) & \mathbf{0}_{2\times n_r} & \mathbf{\Phi}_{CC}(t, t_0)\end{bmatrix},$$

where

$$\begin{aligned}
&\mathbf{\Phi}_{AA}(t, t_0) = \begin{bmatrix}\mathbf{I} & -(t-t_0)\mathbf{I}\\ \mathbf{0} & \mathbf{I}\end{bmatrix},\\
&\mathbf{\Phi}_{BA}(t, t_0) = \begin{bmatrix}\mathbf{\Phi}_{BA1}(t, t_0) & \mathbf{\Phi}_{BA2}(t, t_0)\end{bmatrix},\\
&\mathbf{\Phi}_{BA1}(t, t_0) =\\
&\int_{t_0}^{t} \mathbf{D}_\Upsilon^{-1}(\sigma)\left[\mathbf{U_r}\mathcal{S}\left(\omega(\sigma)\right)\mathcal{R}^T(\sigma) - \mathbf{u}^T(\sigma)\otimes\mathbf{1}_{n_r\times 1}\right]d\sigma,\\
&\mathbf{\Phi}_{BA2}(t, t_0) =\\
&\int_{t_0}^{t} \mathbf{D}_\Upsilon^{-1}(\sigma)\left[\mathbf{U_r}\mathcal{R}^T(\sigma) + \mathbf{u}^{T\,[1]}(\sigma, t_0)\otimes\mathbf{1}_{n_r\times 1}\right]d\sigma -\\
&\int_{t_0}^{t} (\sigma - t_0)\mathbf{D}_\Upsilon^{-1}(\sigma)\left[\mathbf{U_r}\mathcal{S}\left(\omega(\sigma)\right)\mathcal{R}^T(\sigma) - \mathbf{u}^T(\sigma)\otimes\mathbf{1}_{n_r\times 1}\right]d\sigma,
\end{aligned}$$

$$\begin{aligned}
&\mathbf{u}^{[1]}(t, t_0) = \int_{t_0}^{t}\mathbf{u}(\sigma)d\sigma,\\
&\mathbf{\Phi}_{BC}(t, t_0) = \begin{bmatrix}\mathbf{\Phi}_{BC1}(t, t_0) & \mathbf{\Phi}_{BC2}(t, t_0)\end{bmatrix},\\
&\mathbf{\Phi}_{BC1}(t, t_0) = -\int_{t_0}^{t}\boldsymbol{\Upsilon}^{-1}(\sigma)d\sigma,
\end{aligned}$$

and

$$\mathbf{\Phi}_{BC2}(t, t_0) = \int_{t_0}^{t}(\sigma - t_0)\boldsymbol{\Upsilon}^{-1}(\sigma)d\sigma, \tag{15}$$

where the operator $\otimes$ represents the Kronecker product, and $\mathbf{\Phi}_{CA}(t, t_0)$ and $\mathbf{\Phi}_{CC}(t, t_0)$ are omitted as they are not required in the sequel.

Before proceeding with the observability analysis, the following assumption is introduced which ultimately asserts the minimal number of receivers and configuration requirements of the USBL array in order to render the system observable regardless of the trajectory described by the vehicle.

Assumption 3 *There are at least 4 non-coplanar receivers.*

The following theorem establishes the observability of the LTV system (13).

Theorem 4 *The linear time-varying system* (13) *is observable on* $[t_0, t_f]$, $t_0 < t_f$.

Proof *The observability proof of the LTV system* (13) *is accomplished by contradiction. Thus suppose that* (13) *is not observable on* $\mathcal{I} := [t_0, t_f]$*. Then, there exists a non null vector* $\mathbf{d} \in \mathbb{R}^{8+n_r}$

$$\mathbf{d} = \begin{bmatrix} \mathbf{d}_1^T & \mathbf{d}_2^T & \mathbf{d}_3^T & d_4 & d_5 \end{bmatrix}, \tag{16}$$

with $\mathbf{d}_1 \in \mathbb{R}^3$*,* $\mathbf{d}_2 \in \mathbb{R}^3$*,* $\mathbf{d}_3 \in \mathbb{R}^{n_r}$*,* $d_4, d_5 \in \mathbb{R}$*, such that* $\mathbf{d}^T \mathcal{W}(t_0, t_f)\mathbf{d} = 0$ *for all* $t \in \mathcal{I}$*, or equivalently,*

$$\int_{t_0}^{t} \|\mathbf{C}(\tau)\mathbf{\Phi}(\tau, t_0)\mathbf{d}\|^2 d\tau = 0, \quad \forall_{t \in \mathcal{I}}. \tag{17}$$

Taking the time derivative of (17) *gives*

$$\mathbf{C}(t)\mathbf{\Phi}(t, t_0)\mathbf{d} = 0, \quad \forall_{t \in \mathcal{I}}. \tag{18}$$

From (18)*, at* $t = t_0$ *comes*

$$\begin{bmatrix} \mathbf{C}_0\mathbf{d}_3 \\ \mathbf{C}_1(t_0)\mathbf{d}_1 + \mathbf{C}_2\mathbf{d}_3 \end{bmatrix} = \mathbf{0}, \tag{19}$$

which immediately implies that $\mathbf{C}_0\mathbf{d}_3 = \mathbf{0}$*. Since* $\mathbf{C}_0$ *is not singular comes that the only solution is the null vector* $\mathbf{d}_3 = \mathbf{0}$*. Replacing* $\mathbf{d}_3 = \mathbf{0}$ *in* (19) *yields*

$$2\mathbf{D}_{\rho+}^{-1}(t_0)\mathbf{C_2}\mathbf{U_r}\mathcal{R}^T(t_0)\mathbf{d}_1 = \mathbf{0}. \tag{20}$$

Under Assumption 3 the only solution for (20) *is* $\mathbf{d}_1 = \mathbf{0}$*. From* (18) *comes that*

$$\mathbf{C_0}\mathbf{\Phi}_{BA2}(t, t_0)\mathbf{d}_2 + \mathbf{C_0}\mathbf{\Phi}_{BC}(t, t_0)\begin{bmatrix} d_4 \\ d_5 \end{bmatrix} = \mathbf{0}. \tag{21}$$

Taking the time derivative of (21) *allows to write*

$$\begin{aligned} &\mathbf{C_0}\left(\mathbf{D}_\Upsilon^{-1}(t)\left[\mathbf{U_r}\mathcal{R}^T(t) + \mathbf{u}^{T\,[1]}(t, t_0) \otimes \mathbf{1}_{n_r \times 1}\right] + \right. \\ &\left.(t - t_0)\dot{\mathbf{D}}_\Upsilon^{-1}(\sigma)\left[\mathbf{U_r}\mathcal{S}\left(\omega(t)\right)\mathcal{R}^T(t) - \mathbf{u}^T(t) \otimes \mathbf{1}_{n_r \times 1}\right]\right)\mathbf{d}_2 \\ &- \mathbf{C_0}\mathbf{\Upsilon}^{-1}(t)d_4 + (t - t_0)\mathbf{C_0}\dot{\mathbf{\Upsilon}}^{-1}(t)d_5 = \mathbf{0}. \end{aligned} \tag{22}$$

Evaluating (22) *at* $t = t_0$ *yields*

$$\mathbf{C_0}\left[\mathbf{D}_\Upsilon^{-1}(t_0)\mathbf{U_r} \mid -\mathbf{\Upsilon}^{-1}(t_0)\right]\begin{bmatrix} \mathcal{R}^T(t_0)\mathbf{d}_2 \\ d_4 \end{bmatrix} = \mathbf{0}. \tag{23}$$

Under Assumption 3, it is easy to verify in (23)*, that the matrix* $\mathbf{C_0}\left[\mathbf{D}_\Upsilon^{-1}(t_0)\mathbf{U_r} \mid -\mathbf{\Upsilon}^{-1}(t_0)\right]$ *has full rank and therefore the only solution for* (23) *is* $\mathbf{d}_2 = \mathbf{0}$ *and* $d_4 = 0$*. Finally, setting* $\mathbf{d}_1 = \mathbf{0}$*,* $\mathbf{d}_2 = \mathbf{0}$*,* $\mathbf{d}_3 = \mathbf{0}$ *and* $d_4 = 0$ *in* (22) *yields*

$$(t - t_0)\mathbf{C_0}\dot{\mathbf{\Upsilon}}^{-1}(t_0)d_5 = \mathbf{0}. \tag{24}$$

Again the only possible solution for (24) *is* $d_5 = 0$*. This concludes the proof as the only solution* $\mathbf{d} = \mathbf{0}$ *of* (17) *contradicts the hypothesis of the existence of a non null vector* $\mathbf{d}$ *such that* (17) *is true. Thus, by contradiction, the LTV system* (13) *is observable.*

The reasoning behind the need to have at least 4 non-coplanar receivers is that this is the minimum number of receivers so that it is not possible to define a plane that contains all receivers. If a plane that contains all receivers could be defined there would always be at least two possible solutions for the position of the vehicle that satisfy the range measurements. With 4 non-coplanar receivers, the solution for $\mathbf{r}(t)$ is unique.

Although the observability of the LTV system (13) has been established, it does not mean that the original nonlinear system (6) is also observable, because in the proposed augmented LTV structure there is nothing imposing (5) neither the nonlinear algebraic relations between the original and additional states, and neither means that an observer for (13) is also an observer for (6). This however turns out to be true, as it is shown in the next theorem.

Theorem 5 *The nonlinear system* (8) *is observable in the sense that, given* $\{\mathbf{y}(t), t \in [t_0, t_f]\}$ *and* $\{\mathbf{u}(t), t \in [t_0, t_f]\}$*, the initial state* $\mathbf{x}(t_0) = \begin{bmatrix} \mathbf{x}_1^T(t_0) & \mathbf{x}_2^T(t_0) \end{bmatrix}^T$ *is uniquely defined. Moreover, a state observer for the LTV system* (13) *with globally asymptotically stable error dynamics is also a state observer for the nonlinear system* (8)*, with globally asymptotically stable error dynamics.*

Proof *The observability of the LTV system* (13) *has already been established in Theorem 4, thus given* $\{\mathbf{y}(t),\ t \in [t_0, t_f]\}$ *and* $\{\mathbf{u}(t),\ t \in [t_0, t_f]\}$*, the initial state of* (13) *is uniquely defined. Let* $\mathbf{z}(t_0) = \begin{bmatrix} \mathbf{z}_1^T(t_0) & \mathbf{z}_2^T(t_0) & \mathbf{z}_3^T(t_0) & z_4(t_0) & z_5(t_0) \end{bmatrix}^T$ *with* $\mathbf{z}_1(t_0), \mathbf{z}_2(t_0) \in \mathbb{R}^3$*,* $\mathbf{z}_3(t_0) \in \mathbb{R}^{n_r}$*, and* $z_4(t_0), z_5(t_0) \in \mathbb{R}$ *be the initial state of the LTV system* (13) *and* $\mathbf{x}(t_0) = \begin{bmatrix} \mathbf{x}_1^T(t_0) & \mathbf{x}_2^T(t_0) \end{bmatrix}^T$ *be the initial state of the nonlinear system* (8)*. Evaluating the outputs of the augmented system* (13) *at* $t = t_0$*, comes from* (12) *that*

$$\frac{2(\mathbf{b}_i - \mathbf{b}_j)^T\mathcal{R}^T(t_0)\mathbf{z}_1(t_0)}{\rho_i(t_0) + \rho_j(t_0)} + z_{2+i}(t_0) - z_{2+j}(t_0) = \frac{\|\mathbf{b}_i\|^2 - \|\mathbf{b}_j\|^2}{\rho_i(t_0) + \rho_j(t_0)}, \tag{25}$$

Now, noticing that the initial augmented states $z_{2+i}(t_0)$ *with* $i = 1, \ldots, n_r$ *of the LTV system* (13)*, are actually measured, immediately comes that* $z_{2+i}(t_0) = \rho_i(t_0),\ i = 1, \ldots, n_r$*, which used in* (25) *yields*

$$2(\mathbf{b}_i - \mathbf{b}_j)^T\mathcal{R}^T(t_0)\mathbf{z}_1(t_0) + \rho_i^2(t_0) - \rho_j^2(t_0) = \|\mathbf{b}_i\|^2 - \|\mathbf{b}_j\|^2 \tag{26}$$

Setting the actual measured output from (8) *at* $t = t_0$*,* $\rho_i(t_0) = \|\mathbf{b}_i - \mathcal{R}^T(t_0)\mathbf{x_1}(t_0)\|$*, in* (26)*, comes*

$$2(\mathbf{b}_i - \mathbf{b}_j)^T\mathcal{R}^T(t_0)\left[\mathbf{z}_1(t_0) - \mathbf{x}_1(t_0)\right] = 0$$

for all $i, j = 1, \ldots, n_r$, or in compact form

$$\mathbf{C_2 U_r} \mathcal{R}^T(t_0) \left[\mathbf{x}_1(t_0) - \mathbf{z}_1(t_0)\right] = \mathbf{0}. \tag{27}$$

Under Assumption 3 the only solution of (27) *becomes* $\mathbf{x}_1(t_0) = \mathbf{z}_1(t_0)$*, which also trivially asserts that* $z_{2+i}(t_0) = \|\mathbf{z}_1(t_0) - \mathcal{R}(t_0)\mathbf{b}_i\|$*, for all* $i = 1, \ldots, n_r$*. The evolution of* $\mathbf{x}_1(t)$ *for the nonlinear system* (8) *can be easily shown to be given by*

$$\mathbf{x}_1(t) = \mathbf{x}_1(t_0) - (t - t_0)\mathbf{x}_2(t_0) - \mathbf{u}^{[1]}(t, t_0), \tag{28}$$

which is similar to the evolution of $\mathbf{z}_1(t)$ *for the LTV system differing only in the initial condition. Using* (28)*, the output of the nonlinear system* (8) *can be shown to satisfy*

$$\begin{aligned}\rho_i^2(t) =& \|\mathbf{x}_1(t_0) - \mathcal{R}(t_0)\mathbf{b}_i\|^2 - 2\mathbf{x}_1^T(t_0)\mathcal{R}(t)\mathbf{b}_i \\ &+ (t - t_0)^2\|\mathbf{x}_2(t_0)\|^2 + 2\mathbf{x}_1^T(t_0)\mathcal{R}(t_0))\mathbf{b}_i \\ &- 2(t - t_0)\mathbf{x}_2^T(t_0)\mathbf{x}_1(t_0) + 2(t - t_0)\mathbf{x}_2^T(t_0)\mathcal{R}(t)\mathbf{b}_i \\ &+ 2(t - t_0)\mathbf{x}_2^T(t_0)\mathbf{u}^{[1]}(t, t_0) - 2\mathbf{u}^{T\,[1]}(t, t_0)\mathbf{x}_1(t_0) \\ &+ 2\mathbf{u}^{T\,[1]}(t, t_0)\mathcal{R}(t)\mathbf{b}_i + \|\mathbf{u}^{[1]}(t, t_0)\|^2, \end{aligned} \tag{29}$$

and the squared range difference between receiver i *and* j

$$\begin{aligned}&\rho_i^2(t) - \rho_j^2(t) = 2(\mathbf{b}_i - \mathbf{b}_j)^T\mathcal{R}^T(t_0)\mathbf{x}_1(t_0) \\ &- 2(\mathbf{b}_i - \mathbf{b}_j)^T\mathcal{R}^T(t)(\mathbf{x}_1(t_0) - (t - t_0)\mathbf{x}_2(t_0) - \mathbf{u}^{[1]}(t, t_0)) \\ &+ \|\mathbf{x}_1(t_0) - \mathcal{R}(t_0)\mathbf{b}_i\|^2 - \|\mathbf{x}_1(t_0) - \mathcal{R}(t_0)\mathbf{b}_j\|^2. \end{aligned} \tag{30}$$

The squared range of the LTV system (13) *can be shown to satisfy*

$$\begin{aligned}\rho_i^2(t) =& z_{2+i}^2(t_0) - 2\mathbf{z}_1^T(t_0)\mathcal{R}(t)\mathbf{b}_i \\ &+ (t - t_0)^2 z_{n_r+4}(t_0) + 2\mathbf{z}_1^T(t_0)\mathcal{R}(t_0)\mathbf{b}_i \\ &- 2(t - t_0)z_{n_r+3}(t_0) + 2(t - t_0)\mathbf{z}_2^T(t_0)\mathcal{R}(t)\mathbf{b}_i \\ &+ 2(t - t_0)\mathbf{z}_2^T(t_0)\mathbf{u}^{[1]}(t, t_0) - 2\mathbf{u}^{T\,[1]}(t, t_0)\mathbf{z}_1(t_0) \\ &+ 2\mathbf{u}^{T\,[1]}(t, t_0)\mathcal{R}(t)\mathbf{b}_i + \|\mathbf{u}^{[1]}(t, t_0)\|^2, \end{aligned} \tag{31}$$

and consequently it is true, for the LTV system (13)*, that*

$$\begin{aligned}&\rho_i^2(t) - \rho_j^2(t) = z_{2+i}^2(t_0) - z_{2+j}^2(t_0) \\ &- 2(\mathbf{b}_i - \mathbf{b}_j)^T\mathcal{R}^T(t)\left(\mathbf{z}_1(t_0) - (t - t_0)\mathbf{z}_2(t_0) - \mathbf{u}^{[1]}(t, t_0)\right) \\ &+ 2(\mathbf{b}_i - \mathbf{b}_j)^T\mathcal{R}^T(t_0)\mathbf{z}_1(t_0). \end{aligned} \tag{32}$$

Given the solutions for the initial conditions so far and comparing the difference between square of ranges for both systems in (30) *and* (32) *yields*

$$2(t - t_0)(\mathbf{b}_i - \mathbf{b}_j)^T\mathcal{R}^T(t)\left[\mathbf{x}_2(t_0) - \mathbf{z}_2(t_0)\right] = \mathbf{0}. \tag{33}$$

Taking the time derivative of (33) *comes*

$$\begin{aligned}&[-2(t - t_0)(\mathbf{b}_i - \mathbf{b}_j)^T\mathcal{S}\left(\omega(t)\right)\mathcal{R}^T(t) \\ &+2(\mathbf{b}_i - \mathbf{b}_j)^T\mathcal{R}^T(t)]\left(\mathbf{x}_2(t_0) - \mathbf{z}_2(t_0)\right) = \mathbf{0}. \end{aligned} \tag{34}$$

At $t = t_0$ *comes that, for all the possible combinations,* (34) *can be written as*

$$\mathbf{C_2 U_r} \mathcal{R}^T(t_0) \left[\mathbf{x}_2(t_0) - \mathbf{z}_2(t_0)\right] = \mathbf{0}. \tag{35}$$

Again under Assumption 3 the only solution of (35) *is* $\mathbf{x}_2(t_0) = \mathbf{z}_2(t_0)$*. Finally, setting the previous solutions for the initial states in* (31) *and comparing to* (29) *yields*

$$\begin{aligned}&- 2(t - t_0)\left(\mathbf{x}_2^T(t_0)\mathbf{x}_1(t_0) - z_{n_r+3}(t_0)\right) \\ &+ (t - t_0)^2\left(\|\mathbf{x}_2(t_0)\|^2 - z_{n_r+4}(t_0)\right) = \mathbf{0}. \end{aligned} \tag{36}$$

As $(t - t_0)$ *and* $(t - t_0)^2$ *are linearly independent functions, the only solution for* (36) *is* $z_{n_r+3}(t_0) = \mathbf{x}_2^T(t_0)\mathbf{x}_1(t_0)$ *and* $z_{n_r+4}(t_0) = \|\mathbf{x}_2(t_0)\|^2$*. Thus, the initial state of the nonlinear system* (8) *matches the initial state of the LTV system* (13)*, which is uniquely defined. Therefore the nonlinear system* (8) *is also observable.*

Note that the usual concept of observability for nonlinear systems is not as strong as that presented in the statement of Theorem 5, see [12]. Although the observability results were derived with respect to the nonlinear system (8), they also apply to the original nonlinear system (6) as they are related through a Lyapunov transformation. To summarize:

(i) a Lyapunov transformation is applied to the original nonlinear system (8), which preserves all observability properties;
(ii) a LTV system is derived by identifying the nonlinear parts in the sensor measurements kinematics and appropriate state augmentation originating the system in (13);
(iii) the LTV system (13) is shown to be observable in Theorem 4, in the sense that, given the inputs $\mathbf{u}(t)$ and outputs $\mathbf{y}(t)$ in a time interval $[t_0, t_f]$, the initial state $\mathbf{z}(t_0)$ of (13) is uniquely defined;
(iv) the nonlinear system (6) is also shown to be observable in Theorem 5, in the sense that, given the same inputs $\mathbf{u}(t)$ and outputs $\mathbf{y}(t)$ as previously in (iii), the initial state $\mathbf{x}(t_0)$ of (8) is also uniquely defined and, most importantly, it matches the initial state $\mathbf{z}(t_0)$ of (13);
(v) Thus, even though there is nothing imposing the algebraic restrictions between the original states and the augmented states in (13), the systems (8) and (13) are equivalent in the sense that, given the inputs $\mathbf{u}(t)$ and outputs $\mathbf{y}(t)$ in a time interval $[t_0, t_f]$, the initial states of both systems match and are uniquely defined.

Thus, the design of an observer for the original nonlinear system follows simply by reversing the state transformation (7), as it will be detailed in the following section.

3.4 Kalman filter

The augmented structure devised so far was based on a deterministic setting providing strong constructive results, in

the sense that it was shown, in Theorem 5, that an observer with globally asymptotically stable error dynamics for the LTV system (13) provides globally asymptotically stable error dynamics for the estimation of the state of the original nonlinear system. However, in practice there exists measurement noise and system disturbances, motivating the derivation of a filtering solution that accounts for these stochastic quantities. Therefore, the design of a LTV Kalman Filter (even tough other filtering solutions could be used, e.g. a $\mathcal{H}_\infty$ filter) is presented next. Before proceeding with the derivation of the proposed filtering setup, it is important to stress, however, that this filter is not optimal, as the existence of multiplicative noise is evident by looking into the LTV system matrices.

Nevertheless, the Kalman filter has GAS estimation error dynamics, as it can be shown that the system is not only observable but also uniformly completely observable, a sufficient condition for the stability of the LTV Kalman filter [1]. The following technical result is required in the sequel.

Lemma 6 ([3, Lemma 1]) *Let $\mathbf{f}(t) : [t_0, t_f] \subset \mathbb{R} \rightarrow \mathbb{R}^n$ be a continuous and two times continuously differentiable function on $\mathcal{I} := [t_0, t_f]$, $T := t_f - t_0 > 0$, and such that $\mathbf{f}(t_0) = \mathbf{0}$. Further assume that $\max_{t\in\mathcal{I}} \|\ddot{\mathbf{f}}(t)\| \leq C$. If there exists a constant $\alpha^* > 0$ and a time $t^* \in \mathcal{I}$ such that $\|\dot{\mathbf{f}}(t^*)\| \geq \alpha^*$, then there exists constants $\beta^* > 0$ and $0 < \delta^* \leq T$ such that $\|\mathbf{f}(t_0 + \delta^*)\| \geq \beta^*$.*

The following assumption is introduced to guarantee the uniform complete observability of the system.

Assumption 7 *The position of the transponder in the vehicle coordinate frame $\mathbf{r}(t)$, and the angular and linear velocities, $\omega(t)$ and $\mathbf{v}(t)$ respectively, are bounded signals. Moreover, the time derivatives of these signals ($\dot{\mathbf{r}}(t)$, $\dot{\omega}(t)$, and $\dot{\mathbf{v}}(t)$ respectively), are also bonded and the derivatives of the ranges $\dot{\rho}_i(t)$, with $i = 1, \ldots, n_r$ are also bounded.*

From a practical point of view, Assumption 7 is not restrictive since the systems presented herein are in fact finite energy systems that ensemble physical vehicles and sensors. The LTV system (13) is finally shown to be uniformly completely observable in the following theorem.

Theorem 8 *The linear time-varying system* (13) *is uniformly completely observable, that is, there exists positive constants α_1, α_2, δ, such that $\alpha_1\mathbf{I} \preceq \mathcal{W}(t, t+\delta) \preceq \alpha_2\mathbf{I}$ for all $t \geq t_0$.*

Proof *The bounds on the observability Gramian $\mathcal{W}(t, t+\delta)$ can be written as*

$$\alpha_1 \leq \mathbf{d}^T\mathcal{W}(t, t+\delta)\mathbf{d} \leq \alpha_2 \tag{37}$$

for all $t \geq t_0$, and for all $\mathbf{d} \in \mathbb{R}^{8+n_r}$ such that $\|\mathbf{d}\| = 1$. The proof follows by noticing that (37) *can be written as $\alpha_1 \leq \int_t^{t+\delta} \|\mathbf{f}(\tau)\|^2 d\tau \leq \alpha_2$, where*

$$\mathbf{f}(\tau) := \mathbf{C}(\tau)\mathbf{\Phi}(\tau, t)\mathbf{d}. \tag{38}$$

The existence of the upper bound α_2 is trivially checked, as under Assumption 7 the matrices $\mathbf{A}(t)$ and $\mathbf{C}(t)$ are norm-bounded and $\mathbf{f}(\tau)$ is integrated over limited intervals. Let $\mathbf{d} = \begin{bmatrix}\mathbf{d}_1^T & \mathbf{d}_2^T & \mathbf{d}_3^T & d_4 & d_5\end{bmatrix}$, with $\mathbf{d}_1 \in \mathbb{R}^3$, $\mathbf{d}_2 \in \mathbb{R}^3$, $\mathbf{d}_3 \in \mathbb{R}^{n_r}$, $d_4, d_5 \in \mathbb{R}$. Evaluating (38) *at $\tau = t$, it is straightforward to verify that if $\mathbf{d}_3 \neq \mathbf{0}$, then $\|\mathbf{f}(t)\|$ is immediately bounded. Indeed, as $\|\mathbf{f}(t)\| \geq \|\mathbf{C_0}\mathbf{d}_3\| = \alpha_1^* > 0$ for all $t \geq t_0$, since $\mathbf{C_0}$ has full column rank by construction. Suppose now that $\mathbf{d}_3 = \mathbf{0}$. Then, it can also be seen that if $\mathbf{d}_1 \neq \mathbf{0}$, it is true that $\|\mathbf{f}(t)\| = \|\mathbf{C_1}(t)\mathbf{d}_1\|$, or, using* (14)*,*

$$\|\mathbf{f}(t)\| = \|2\mathbf{D}_{\rho+}^{-1}(t)\mathbf{C_2}\mathbf{U_r}\mathcal{R}^T(t)\mathbf{d}_1\|, \tag{39}$$

which is clearly bounded by

$$\|\mathbf{f}(t)\| \geq \sigma_{min}(\mathbf{D}_{\rho+}^{-1}(t))\|2\mathbf{C_2}\mathbf{U_r}\mathcal{R}^T(t)\mathbf{d}_1\| \tag{40}$$

for all $t \geq t_0$, where the operator $\sigma_{min}(\mathbf{A})$ represents the smallest singular value of $\mathbf{A}$. Under Assumption 2 it is clear that $\sigma_{min}(\mathbf{D}_{\rho+}^{-1}(t)) \geq \frac{1}{R_{max}}$ for all $t \geq t_0$, which implies

$$\|\mathbf{f}(t)\| \geq \frac{1}{R_{max}}\sigma_{min}(\mathbf{C_2}\mathbf{U_r})\left\|\mathcal{R}^T(t)\mathbf{d}_1\right\|$$

for all $t \geq t_0$. Now under Assumption 3 it follows that $\mathbf{C_2}\mathbf{U_r}$ has full column rank and therefore there exists a positive constant β_1^* such that $\sigma_{min}(\mathbf{C_2}\mathbf{U_r}) = \beta_1^* > 0$. Thus, taking into account that $\left\|\mathcal{R}^T(t)\mathbf{d}_1\right\| = \|\mathbf{d}_1\|$,

$$\|\mathbf{f}(t)\| \geq \frac{\beta_1^*}{R_{max}}\|\mathbf{d}_1\| = \alpha_2^* > 0 \tag{41}$$

for all $t \geq t_0$. Using the same set of assumptions and procedures it is possible to show that the derivative of $\mathbf{f}(\tau)$ evaluated at $\tau = t$ is also uniformly bounded

$$\left\|\frac{\partial\mathbf{f}(\tau)}{\partial\tau}\Big|_{\tau=t}\right\| \geq \frac{\beta_2^*\beta_3^*}{R_{max}}\left\|\begin{bmatrix}\mathbf{d_2}\\ d_4\end{bmatrix}\right\| = \alpha_3^* > 0, \tag{42}$$

for all $t \geq t_0$, with β_2^* and β_3^* positive constants, and when $\mathbf{d}_3 = \mathbf{0}$, $\mathbf{d}_1 = \mathbf{0}$ and either $\mathbf{d}_2 \neq \mathbf{0}$ or $d_4 \neq 0$. The upper boundedness on the norm of the second derivative of $\mathbf{f}(\tau)$ becomes straightforward under Assumption 7, thus allowing the use of Lemma 6 in (42)*. Thus, in this case, it can be shown, using Lemma 6, that there exist $\alpha_4^* > 0$ and $\delta_1^* > 0$ such that $\|\mathbf{f}(t + \delta_1^*)\| \geq \alpha_4^*$ for all $t \geq t_0$. Using Lemma 6 again, there exist positive constants $\alpha_5^* > 0$ and $\delta^* > 0$ such that*

$$\mathbf{d}^T\mathcal{W}(t, t+\delta^*)\mathbf{d} \geq \alpha_5^*, \tag{43}$$

for all $t \geq t_0$ and when $\mathbf{d_1} = \mathbf{0}$, $\mathbf{d_3} = \mathbf{0}$, and $\mathbf{d_2} \neq \mathbf{0}$ or $d_4 \neq 0$. When all the components of $\mathbf{d}$ are null except d_5 it

follows that

$$\mathbf{f}(\tau) = \begin{bmatrix} \mathbf{C_0}\Phi_{BC2}(\tau,t)d_5 \\ \mathbf{C_2}\Phi_{BC2}(\tau,t)d_5 \end{bmatrix}, \tag{44}$$

which norm is clearly bounded by

$$\|\mathbf{f}(\tau)\| \geq \sigma_{min}(\mathbf{C_0})\,\|\mathbf{\Phi}_{BC2}(\tau,t)d_5\| \tag{45}$$

for all $t \geq t_0$. Expanding (45) *and using* (15) *yields*

$$\|\mathbf{f}(\tau)\| \geq \beta_2^* \sqrt{\sum_{i=1}^{n_r} \left(d_5 \int_t^{\tau} \frac{\sigma - t}{\rho_1(\sigma)} d\sigma \right)^2} \tag{46}$$

for all $t \geq t_0$. In particular at $\tau = t + \delta_2^*$, with $\delta_2^* > 0$, comes

$$\|\mathbf{f}(t+\delta_2^*)\| \geq \beta_2^* |d_5| \sqrt{\sum_{i=1}^{n_r} \left(\int_t^{t+\delta_2^*} \frac{\sigma - t}{\rho_i(\sigma)} d\sigma \right)^2} \tag{47}$$

for all $t \geq t_0$. By the Integral Mean Value theorem there exists $c \in]t, t+\delta_2^*[$ such that

$$\int_t^{t+\delta_2^*} \frac{\sigma - t}{\rho_1(\sigma)} d\sigma = \delta_2^* \frac{c - t}{\rho_i(c)}. \tag{48}$$

for all $t \geq t_0$. Now defining $\delta_3^* := c - t > 0$, which is clearly positive because $c > t$, allows to write

$$\int_t^{t+\delta_2^*} \frac{\sigma - t}{\rho_1(\sigma)} d\sigma = \frac{\delta_2^* \delta_3^*}{\rho_i(t+\delta_3^*)}. \tag{49}$$

for all $t \geq t_0$. Under Assumption 2 comes from (47) *and* (49) *that*

$$\begin{aligned} \|\mathbf{f}(t+\delta_2^*)\| &\geq \beta_2^* |d_5| \sqrt{\sum_{i=1}^{n_r} \left(\frac{\delta_2^* \delta_3^*}{R_{max}} \right)^2} \\ &= \frac{\delta_2^* \delta_3^* \beta_2^* |d_5| \sqrt{n_r}}{R_{max}} = \alpha_6^* > 0 \end{aligned} \tag{50}$$

for all $t \geq t_0$. Finally, Lemma 6 is used once again to show that there exist $\alpha > 0$ and $\delta > 0$, for all $t \geq t_0$ and $\{\mathbf{d} \in \mathbb{R}^{8+n_r} : \|\mathbf{d}\| = 1\}$, such that $\mathbf{d}^T \mathcal{W}(t, t+\delta)\mathbf{d} \geq \alpha$, which means that the system is uniformly completely observable and therefore concludes the proof.

To recover the augmented system dynamics in the original coordinate space, the original Lyapunov state transformation (7) is reverted considering the augmented state transformation $\mathbf{\Gamma}(t) := \mathbf{T_r}^T(t)\mathbf{x}(t)$, where $\mathbf{T_r}(t) := \text{diag}\,(\mathcal{R}(t), \mathcal{R}(t), 1, \ldots, 1)$ is a also Lyapunov state transformation that preserves all observability properties of the LTV system (13). Thus, the reverted augmented dynamics are given by

$$\begin{cases} \dot{\mathbf{\Gamma}}(t) = \mathbf{A_\Gamma}(t)\mathbf{\Gamma}(t) + \mathbf{B_\Gamma}(t)\mathbf{v_r}(t), \\ \mathbf{y}(t) = \mathbf{C_\Gamma}(t)\mathbf{\Gamma}(t), \end{cases} \tag{51}$$

where

$$\mathbf{A_\Gamma}(t) = \begin{bmatrix} -\mathcal{S}(\omega(t)) & -\mathbf{I} & \mathbf{0} & \mathbf{0} & \mathbf{0} \\ \mathbf{0} & -\mathcal{S}(\omega(t)) & \mathbf{0} & \mathbf{0} & \mathbf{0} \\ \frac{\mathbf{b}_1^T \mathcal{S}(\omega(t)) - \mathbf{v_r}^T(t)}{\rho_1(t)} & \frac{\mathbf{b}_1^T}{\rho_1(t)} & \mathbf{0} & -\frac{1}{\rho_1(t)} & 0 \\ \vdots & \vdots & \vdots & \vdots & \vdots \\ \frac{\mathbf{b}_{n_r}^T \mathcal{S}(\omega(t)) - \mathbf{v_r}^T(t)}{\rho_{n_r}(t)} & \frac{\mathbf{b}_{n_r}^T}{\rho_{n_r}(t)} & \mathbf{0} & -\frac{1}{\rho_{n_r}(t)} & 0 \\ \mathbf{0} & -\mathbf{v_r}^T(t) & \mathbf{0} & 0 & -1 \\ \mathbf{0} & \mathbf{0} & \mathbf{0} & 0 & 0 \end{bmatrix}, \tag{52}$$

$$\mathbf{B_\Gamma}(t) = \begin{bmatrix} -\mathbf{I}_3 & \mathbf{0} & \frac{\mathbf{b}_1}{\rho_1(t)} & \cdots & \frac{\mathbf{b}_{n_r}}{\rho_{n_r}(t)} & \mathbf{0} & \mathbf{0} \end{bmatrix}^T, \tag{53}$$

and

$$\mathbf{C_\Gamma}(t) = \begin{bmatrix} \mathbf{0}_{n_r \times 3} & \mathbf{0}_{n_r \times 3} & \mathbf{C_0} & \mathbf{0}_{n_r \times 2} \\ 2\mathbf{D}_{\rho^+}^{-1}(t)\mathbf{C_2}\mathbf{U_r} & \mathbf{0}_{n_c \times 3} & \mathbf{C_2} & \mathbf{0}_{n_c \times 2} \end{bmatrix}. \tag{54}$$

Including system disturbances and sensor noise in (51) yields the final reverted augmented dynamics

$$\begin{cases} \dot{\mathbf{\Gamma}}(t) = \mathbf{A_\Gamma}(t)\mathbf{\Gamma}(t) + \mathbf{B_\Gamma}(t)\mathbf{v_r}(t) + \mathbf{n_x}(t), \\ \mathbf{y}(t) = \mathbf{C_\Gamma}(t)\mathbf{\Gamma}(t) + \mathbf{n_y}(t), \end{cases} \tag{55}$$

where $\mathbf{n_x}(t)$ and $\mathbf{n_y}(t)$ are assumed to be uncorrelated, zero-mean, white Gaussian noise, with $E\left[\mathbf{n_x}(t)\mathbf{n_x}^T(\tau)\right] = \mathbf{Q_x}(t)\delta(t-\tau)$ and $E\left[\mathbf{n_y}(t)\mathbf{n_y}^T(\tau)\right] = \mathbf{Q_y}(t)\delta(t-\tau)$.

At this stage, is important to remark that the disturbances and sensor noise are included in the reverted system (55) and are not affected by the Lyapunov state transformation (7), which preserves, nonetheless, all observability properties of the original system. The proposed transformation (7) is solely used to obtain the strong observability results presented so far, and the final filtering stage is set on the original state coordinates with an augmented structure. Nevertheless, all the results could have been obtained without the use of the Lyapunov transformation, at the expense of more computations. Due to natural reverberation, surface scattering, reflections on the seabed, surface and other underwater structures, acoustic sensors like the USBL are highly susceptible to multipath which produces outliers on the positioning information. The inclusion of the ranges kinematics in the proposed augmented structure ultimately allows for a more comprehensive description of coloured noise on the acoustic sensor readings. The design framework also enables the

filter to more easily tackle individual range measurements outages by simply bypassing corrections from problematic receivers, whereas in traditional inertial based solutions a position fix might not even be available or unique if one acoustic receiver fails to detect the signal underwater. Although this paper presents the design of a sensor-based Kalman filter with GAS error dynamics, other filtering schemes could be devised, with the same proposed augmented state structure, naturally inheriting the same observability properties. In particular, in order to tackle acoustic outliers, available solutions in the literature include the use of on-line outlier detection and removal schemes as proposed in [16] prior to filtering, and the design of robust Kalman filters that are able to ignore outliers in the observations [10,22].

3.5 Performance bounds analysis

Theoretical performance bounds have long been pursued as an important design tool that helps gauge the attainable performance by any estimator on pre-set conditions of process observations and noise. These kind of bounds allow as well for an assessment of whether imposed performance specifications are feasible or not. A commonly used lower bound for time-invariant statistical models is the Cramér-Rao Bound (CRB), which provides a lower bound on the estimation error of any estimator of an unknown constant parameter of that particular statistical model. An analogous bound for random parameters on non-linear, non-stationary system models, referred to as the Bayesian Cramér-Rao Bound (BCRB), was first derived in [23] and carefully reviewed in [24,25].

The BCRB arises as a valuable analysis tool to assess the performance of dynamical estimators, and it is used in this work to assess the achievable performance of the proposed navigation system. Even tough the natural framework of the filters presented in this paper falls in the scope of more general process models with multiplicative noise due to the presence of the angular rates measurement noise in the filter dynamics, the performance bound analysis is restricted to the case of linear Gaussian process models with additive white noise and nonlinear observation models. Simulation results presented herein with realistic noise in all measured quantities reveal, nonetheless, that the proposed filters operate near the performance bound indicated by the BCRB, whereas the inclusion of the multiplicative noise would only increase and tighten the theoretical performance bound.

Consider the general linear process and nonlinear observation models given by

$$\begin{cases} \dot{\mathbf{x}}(t) = \mathbf{F}(t)\mathbf{x}(t) + \mathbf{B}(t)\mathbf{u}(t) + \mathbf{G}(t)\mathbf{n}_{\mathbf{x}}(t), \\ \mathbf{y}(t) = \mathbf{h}\left(\mathbf{x}(t)\right) + \mathbf{n}_{\mathbf{y}}(t), \end{cases} \tag{56}$$

where $\mathbf{x}(t)$ is the state vector, $\mathbf{u}(t)$ is a deterministic system input, $\mathbf{y}(t)$ is the measurement vector which is related to the state vector by the nonlinear observation model $\mathbf{h}\left(\mathbf{x}(t)\right)$, and $\mathbf{n}_{\mathbf{x}}(t)$ and $\mathbf{n}_{\mathbf{y}}(t)$ represent respectively the state and measurements stochastic perturbations.

The Bayesian bound derived by Snyder in [21] shows that the covariance matrix of any given causal (realizable) unbiased estimate of (56),

$$E\left\{\left(\hat{\mathbf{x}}(t) - \mathbf{x}(t)\right)\left(\hat{\mathbf{x}}(\tau) - \mathbf{x}(\tau)\right)^{T}\right\} = \mathbf{P}(t)\delta(t-\tau), \tag{57}$$

is lower bounded by

$$\mathbf{P}(t) \geq \mathbf{J}_{g}^{-1}(t), \tag{58}$$

where $\mathbf{J}_{g}(t)$ is known as the Fisher Information Matrix (FIM), which satisfies the matrix differential equation

$$\begin{aligned} \dot{\mathbf{J}}_{g} = &-\mathbf{J}_{g}\mathbf{F}(t) - \mathbf{F}^{T}(t)\mathbf{J}_{g} - \mathbf{J}_{g}\mathbf{G}(t)\mathbf{Q}(t)\mathbf{G}^{T}(t)\mathbf{J}_{g} \\ &+ \mathbf{P}_{m}(\mathbf{x}(t), t), \end{aligned} \tag{59}$$

where $\mathbf{Q}(t)$ is the state noise $\mathbf{n}_{\mathbf{x}}(t)$ covariance matrix. The subscript g denotes that the underlying process model is a linear Gaussian model, and the subscript m stands for *measurement*, since the term $\mathbf{P}_{m}(t)$ accounts for the covariance reduction due to the observations and is given by

$$\mathbf{P}_{m}(\mathbf{x}(t), t) = E_{\mathbf{x}}\left\{\tilde{\mathbf{H}}^{T}(\mathbf{x}(t))\mathbf{R}^{-1}\tilde{\mathbf{H}}(\mathbf{x}(t))\right\}, \tag{60}$$

where $\tilde{\mathbf{H}}(\mathbf{x}(t))$ is the Jacobian of the nonlinear observation model evaluated at $\mathbf{x}(t)$, and $\mathbf{R}(t)$ is the measurement noise $\mathbf{n}_{\mathbf{y}}(t)$ covariance matrix.

Note that the expectation in (60) is with respect to the state vector $\mathbf{x}(t)$ and will usually have to be evaluated by a Monte Carlo simulation. In nonlinear tracking problems, as in the framework presented herein, we are often interested in how well we can estimate a specific or nominal track $\bar{\mathbf{x}}(t)$ in which case the term $\mathbf{P}_{m}(\mathbf{x}(t), t)$ can be simplified to

$$\mathbf{P}_{m}(\bar{\mathbf{x}}(t), t) = \tilde{\mathbf{H}}^{T}(\bar{\mathbf{x}}(t))\mathbf{R}^{-1}\tilde{\mathbf{H}}(\bar{\mathbf{x}}(t)), \tag{61}$$

allowing for the assessment of the achievable performance for any tracker or estimator given this specific underlying problem structure. The resulting equations are analogous to the Information filter version of the Extended Kalman Filter, whereas the Jacobians are computed at the nominal $\bar{\mathbf{x}}(t)$ trajectories instead of the estimated trajectories, as convincingly argued in [25]. Depending on the noise intensities, such bound calculated over the nominal trajectory often suffices to quantify performance margins and perform gain adjustments. Note that in the particular case of the present work, the BCRB is computed for the rigid body kinematics model and the nonlinear USBL observation model with

$$\mathbf{F}(t) = \begin{bmatrix} -\mathcal{S}\left(\omega(t)\right) & -\mathbf{I} \\ \mathbf{0} & -\mathcal{S}\left(\omega(t)\right) \end{bmatrix}, \tag{62}$$

$$\mathbf{G}(t) = \mathbf{B}(t) = \begin{bmatrix} -\mathbf{I} & \mathbf{0} \end{bmatrix}^{T}, \tag{63}$$

which model the variables of interest to estimate, instead of being computed for the full augmented system.

4 Numerical Results and Performance Evaluation

The performance of the proposed Linear Time-Varying Kalman Filter (LTVKF) was assessed in simulation using a kinematic model for an underwater vehicle. The vehicle describes a trimming trajectory as depicted in Figure 2.

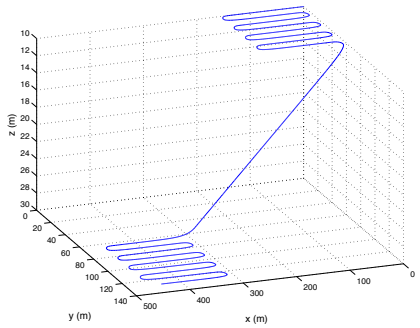

Fig. 2. Vehicle trimming trajectory

The USBL receiving array is composed of 4 receivers that are installed on the vehicle, with an offset of 30 cm along the x-axis of the body-fixed coordinate frame $\{B\}$, where the DVL and the AHRS with the rate gyros are also installed. Thus the positions of the receivers with respect to $\{B\}$ are given in meters by $\mathbf{b}_1 = \begin{bmatrix} 0.2 & -0.15 & 0 \end{bmatrix}^T$, $\mathbf{b}_2 = \begin{bmatrix} 0.2 & 0.15 & 0 \end{bmatrix}^T$, $\mathbf{b}_3 = \begin{bmatrix} 0.4 & 0 & 0.15 \end{bmatrix}^T$, and $\mathbf{b}_4 = \begin{bmatrix} 0.4 & 0 & -0.15 \end{bmatrix}^T$.

The DVL fluid-relative velocity measurements are considered to be corrupted by additive uncorrelated zero-mean white Gaussian noise with an accuracy of 0.2% of the nominal velocity and an additional standard deviation of $1\ mm/s$, which is inspired on the LinkQuest NavQuest 600 Micro$^{\text{TM}}$DVL sensor package. Two AHRS sensor packages are considered for performance evaluation of the proposed solution, also inspired in realistic commercially available units: the first is a high cost, high grade iXSea OCTANS$^{\text{TM}}$AHRS equipped with very good performance Fiber Optic Gyros (FOG) capable of measuring the angular motion of the vehicle with an accuracy of $0.01\ deg/s$, and an overall orientation accuracy of $0.1\ deg$ for the yaw angle, and $0.01\ deg$ for the pitch and roll angles; the latter is a low grade, MEMS based (Micro-Electro-Mechanical Systems), smaller and with a significantly lower price tag, MicroStrain 3DM-GX3-25$^{\text{TM}}$AHRS that outputs the angular motion rates of the vehicle with an accuracy of $0.2\ deg/s$, and that has an overall dynamic orientation accuracy of $2\ deg$.

The range measurements between the transponder and the reference receiver (receiver 1) are considered to be disturbed by additive, zero-mean white Gaussian noise, with $1\ m$ standard deviation whilst the RDOA between receiver 1 and the other 3 receivers is considered to be measured with an accuracy of $6\ mm$. The transponder is located in inertial coordinates at ${}^I\mathbf{p}_t = \begin{bmatrix} 200 & 0 & 0 \end{bmatrix}^T\ [m]$, and the unknown underwater current velocity has an intensity of $0.2\ m/s$ in all three axis.

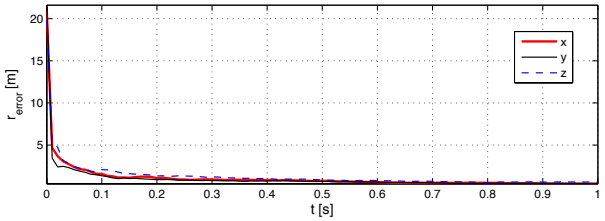

Fig. 3. LTV Kalman filter initial convergence - transponder position RMS estimation error

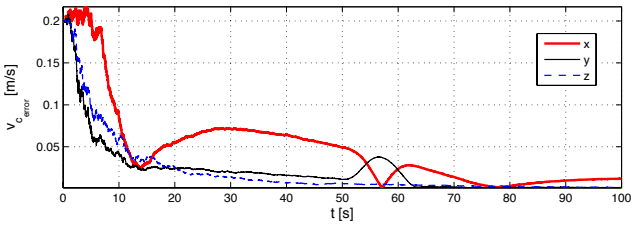

Fig. 4. LTV Kalman filter initial convergence - current velocity RMS estimation error

The assessment of performance of the filter is carried out resorting to Monte Carlo simulations and by comparing the Root-Mean-Square (RMS) estimation error of the filters to the BCRB (computed at the nominal trajectory described by the vehicle). Starting at different initial conditions, the filter is evaluated through 20 Monte Carlo runs and sets of independent random noise. The augmented states that correspond to the ranges $x_3, \ldots, x_{2+n_r}$ are initialized with the first set of measurements available, the initial filter position estimate is drawn from a normal Gaussian distribution with mean equal to the nominal initial position and a standard deviation of $20\ m$, and the remaining initial estimates are set to zero.

With the purpose of evaluating the convergence of the proposed filtering structure in simulation, an initial convergence study is conducted using the angular motion rate measurements from the high grade AHRS. The initial evolution of the position RMS estimation error is depicted in Figure 3, where the fast convergence of the position error is evidenced. The initial evolution of the current velocity RMS estimation error is plotted in Figure 4.

The RMS estimation error on the evolution of the augmented states that correspond to the distances between the receivers and the transponder is represented in Figure 5. The remaining augmented states are also shown to converge correctly in Figure 6.

Using the same batch of Monte Carlo runs, the performance of the proposed filter is compared with two alternative filter

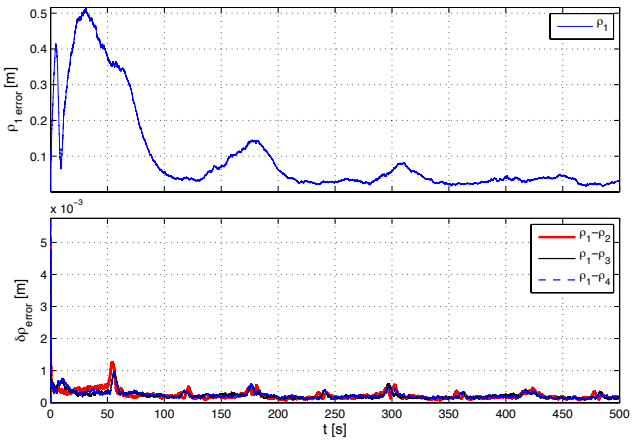

Fig. 5. LTV Kalman filter distances corresponding augmented states evolution - RMS estimation error

designs, the well known and established Extended Kalman Filter (EKF) and the classical approach based on a Kalman filter designed in inertial coordinates and that employs the planar wave approximation to get position fixes. The first design linearizes the nonlinear range and RDOA measurements about the filter estimates in order to compute a suboptimal Kalman gain. In the latter, the feedback is accomplished in inertial coordinates by means of a precomputed transponder position fix from the USBL that resorts to a planar wave approximation, previously used by the authors [17].

Comparing the steady-state response of the three filters using the high grade AHRS in Figure 7, it can be seen that the EKF and the proposed augmented LTVKF attain the same performance level, whereas the classical approach fails to achieve the same performance of the proposed solution and the EKF, as expected and mainly due to the need to convert the measured and estimated quantities back and forth between the body and the inertial frames using the AHRS. The BCRB for the rigid body kinematics and the nonlinear USBL measurements is also shown in Figure 7, allowing to see that the proposed filter and the EKF operate close to the performance lower bound. The error peaks that appear in the steady-state response are due to the high rotational velocity that is achieved during the curves shown in Figure 2.

Comparing the performance of both designs with the lower bound it can be stated that they achieve the same performance level and close to the bound. The solution presented

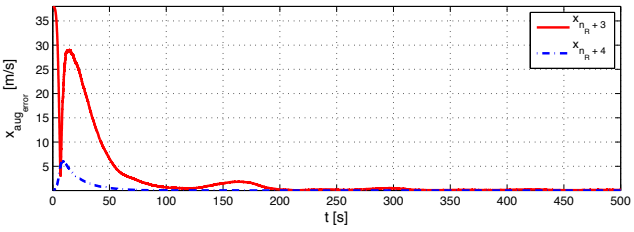

Fig. 6. LTV Kalman filter augmented states evolution - RMS estimation error

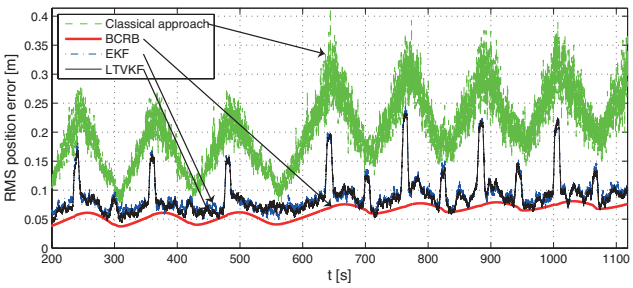

Fig. 7. Comparison of steady state response with performance bound - RMS estimation error with High Grade AHRS

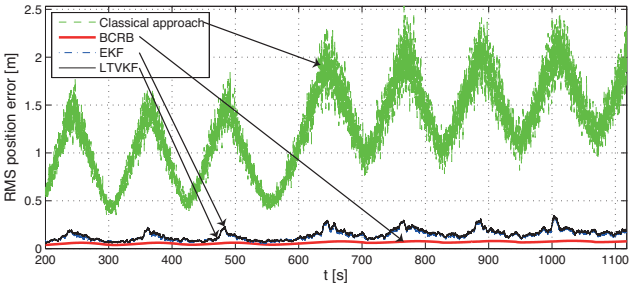

Fig. 8. Comparison of steady state response with performance bound - RMS estimation error with Low Grade AHRS

in this work has the advantage of being GAS, which is not guaranteed for the other designs.

The same performance comparison is conducted using the low grade AHRS, and reported in Figure 8, which clearly emphasizes the performance enhancement of the proposed solution. The performance of the EKF and the LTVKF can be seen to maintain an equivalent performance level while slightly steering away from the BCRB. The performance degradation is nonetheless more severe for the classical strategy.

5 Conclusions

The main contribution of the paper lies on the design of globally asymptotically stable position filters based directly on the sensor readings of an USBL acoustic array and a DVL. At the core of the proposed filtering solution is the derivation of a LTV system that fully captures the dynamics of the nonlinear system. This LTV model is achieved through appropriate state augmentation, allowing for the use of powerful linear system analysis and filtering design tools that yield GAS filter error dynamics. The performance analysis of the proposed filter was carried out resorting to Monte Carlo simulations and compared against the theoretical performance lower bound given by the BCRB and against two traditional solutions, the EKF and a Kalman filter designed on inertial coordinates that resorts to the planar approximation of the acoustic wave arriving at the USBL array.

Comparison of the steady-state position error from the three designs and the BCRB lead to the conclusion that the proposed design demonstrated similar performance level to the EKF using realistic sensor noise and disturbances, while operating tightly to the performance lower bound, and outperforming the classical inertial based design. The utmost advantage of the new filter structure is nevertheless evident, due to its GAS properties which is not guaranteed for either of the two more traditional solutions. Moreover, the inclusion of the ranges kinematics in the proposed augmented structure ultimately allows for a more comprehensive description of coloured noise on the acoustic sensor readings. The design framework also enables the filter to more easily tackle individual range measurements outages by simply bypassing corrections from problematic receivers, whereas in the classical solution a position fix might not even be available or unique if one acoustic receiver fails to detect the signal underwater.

Acknowledgements

This work was supported by FCT (ISR/IST plurianual funding) through the PIDDAC Program funds, and partially funded by EU Project TRIDENT (Contract No. 248497). The work of M. Morgado was supported by a PhD Student Scholarship with reference SFRH/BD/25368/2005, from the Fundação para a Ciência e a Tecnologia.

References

[1] B. Anderson. Stability properties of Kalman-Bucy filters. *Journal of the Franklin Institute*, 291(2):137–144, 1971.

[2] P. J. Antsaklis and A. N. Michel. *Linear systems*. Birkhauser, 2006.

[3] P. Batista, C. Silvestre, and P. Oliveira. Sensor-based Complementary Globally Asymptotically Stable Filters for Attitude Estimation. In *Proceedings of the 48th IEEE Conference on Decision and Control*, pages 7563–7568, Shanghai, China, December 2009.

[4] P. Batista, C. Silvestre, and P. Oliveira. Single Range Navigation in the presence of Constant Unknown Drifts. In *Proceedings of the European Control Conference 2009 - ECC'09*, Budapest, Hungary, August 2009.

[5] P. Batista, C. Silvestre, and P. Oliveira. Optimal position and velocity navigation filters for autonomous vehicles. *Automatica*, 46(4):767–774, April 2010.

[6] R. W. Brockett. *Finite Dimensional Linear Systems*. Wiley, 1970.

[7] S. Celikovsky and G. Chen. Secure synchronization of a class of chaotic systems from a nonlinear observer approach. *IEEE Transactions on Automatic Control*, 50(1):76–82, 2005.

[8] K. D. Do, Z. P. Jiang, J. Pan, and H. Nijmeijer. A global output-feedback controller for stabilization and tracking of underactuated ODIN: A spherical underwater vehicle. *Automatica*, 40(1):117 – 124, 2004.

[9] R. M. Eustice, L. L. Whitcomb, H. Singh, and M. Grund. Experimental results in synchronous-clock one-way-travel-time acoustic navigation for autonomous underwater vehicles. In *Robotics and Automation, 2007 IEEE International Conference on*, pages 4257–4264, 2007.

[10] M.A. Gandhi and L. Mili. Robust Kalman filter based on a generalized maximum-likelihood-type estimator. *Signal Processing, IEEE Transactions on*, 58(5):2509–2520, 2010.

[11] J. C. García, J. F. Fresneda, P. Sanz, and R. Marín. Increasing autonomy within underwater intervention scenarios: The user interface approach. In *2010 IEEE International Systems Conference*, San Diego, CA, USA, 4 2010.

[12] R. Hermann and A. J. Krener. Nonlinear controllability and observability. *IEEE Transactions on Automatic Control*, 22(5):728–740, 1977.

[13] L. Imsland, T. A. Johansen, T. I. Fossen, H. F. Grip, J. C. Kalkkuhl, and A. Suissa. Vehicle velocity estimation using nonlinear observers. *Automatica*, 42(12):2091 – 2103, 2006.

[14] J. C. Kinsey and L. L. Whitcomb. Preliminary field experience with the DVLNAV integrated navigation system for oceanographic submersibles. *Control Engineering Practice*, 12(12):1541–1548, December 2004. Invited Paper.

[15] J. C. Kinsey and L. L. Whitcomb. In situ alignment calibration of attitude and doppler sensors for precision underwater vehicle navigation: Theory and experiment. *IEEE Journal of Oceanic Engineering*, 32(2):286–299, April 2007.

[16] R.K. Menold P.H., Pearson and F. Allgower. Online outlier detection and removal. In *Proceedings of MED99 (7th International Conference on Control and Automation), Haifa, Israel*, pages 1110–1134, 1999.

[17] M. Morgado, P. Oliveira, C. Silvestre, and J.F. Vasconcelos. USBL/INS Tightly-Coupled Integration Technique for Underwater Vehicles. In *Proceedings Of The 9th International Conference on Information Fusion*, Florence, Italy, July 2006. IEEE.

[18] A. Pascoal, P. Oliveira, and C. Silvestre *et al.* Robotic Ocean Vehicles for Marine Science Applications: the European ASIMOV Project. In *Proceedings of the Oceans 2000*, Rhode Island, USA, September 2000.

[19] A. Pisano and E. Usai. Output-feedback control of an underwater vehicle prototype by higher-order sliding modes. *Automatica*, 40(9):1525 – 1531, 2004.

[20] P. Rigby, O. Pizarro, and S.B. Williams. Towards geo-referenced auv navigation through fusion of USBL and DVL measurements. In *OCEANS 2006*, pages 1–6, Sept. 2006.

[21] D. L. Snyder and I. B. Rhodes. Filtering and Control Performance Bounds with Implications on Asymptotic Separation. *Automatica*, pages 747–753, Nov. 1972.

[22] J.A. Ting, E. Theodorou, and S. Schaal. A Kalman filter for robust outlier detection. In *Intelligent Robots and Systems, 2007. IROS 2007. IEEE/RSJ International Conference on*, pages 1514–1519. IEEE, 2007.

[23] H. L. Van Trees. Bounds on the Accuracy Attainable in the Estimation of Continuous Random Processes. *IEEE Transactions on Info. Theory*, 12:298–305, 1966.

[24] H. L. Van Trees. *Detection, estimation, and modulation theory.. part 1,. detection, estimation, and linear modulation theory*. Wiley New York, 1968.

[25] H. L. Van Trees and L. K. Bell. *Bayesian Bounds for Parameter Estimation and Nonlinear Filtering/Tracking*. John Wiley & Sons - IEEE Press, first edition, 2007.

[26] L. L. Whitcomb. Underwater robotics: out of the research laboratory and into the field. In *Robotics and Automation, 2000. Proceedings. ICRA '00. IEEE International Conference on*, volume 1, pages 709–716 vol.1, 2000.

[27] E. Willemenot, P.-Y. Morvan, H. Pelletier, and A. Hoof. Subsea positioning by merging inertial and acoustic technologies. In *OCEANS 2009-EUROPE, 2009. OCEANS '09.*, pages 1–8, May 2009.